

## ACCURACY ANALYSIS OF THE LEICA HDS3000 AND FEASIBILITY OF TUNNEL DEFORMATION MONITORING

Roderik Lindenbergh, Norbert Pfeifer, Tahir Rabbani

Delft Institute of Earth Observation and Space systems, Delft University of Technology  
Kluyverweg 1, 2629 HS Delft, The Netherlands (r.c.lindenbergh, n.pfeifer, t.rabbani)@lr.tudelft.nl

**KEY WORDS:** terrestrial laser scanning, accuracy analysis, change detection

### ABSTRACT:

Deformation monitoring with total stations, while superior in accuracy, suffers from the poor spatial resolution obtainable by this measurement method within the limited time on a tunnel construction site, and deformation can only be detected at previously marked target points. Due to its high speed in obtaining unstructured point clouds from all surfaces within the field of view terrestrial laser scanning can be – at least – complementary in monitoring deformation. In this study we test one of the new panoramic high precision laser scanners (Leica HDS3000) for its feasibility in tunnel deformation monitoring. Accuracy is tested in a tunnel with respect to range and angle of incidence. Not all points measured by the laser scanner can serve for deformation monitoring due to measurement artifacts at edges. We propose to use segmentation for selecting the suitable points only.

### 1 INTRODUCTION

**Terrestrial laser scanning.** A terrestrial laser scanner determines the distance between a large number of object points and the scanner by emitting laser pulses in different directions and detecting the echoes from the objects. So called pulsed scanners measure the travel time of the pulse towards an object and back. This technique therefore uses the intensity of the light signal to detect when an emitted signal returns to the scanner. An overview of measurement techniques and scanner specifications can be found in [Pfeifer and Litchi, 2004].

**Leica HDS3000** The pulsed scanner used in the experiment described here is the Leica HDS3000. The company claims a precision of 6mm at a scan distance of 50m. The maximal scan distance amounts to 100m. The scan range reaches  $270^\circ$  in the vertical direction and is complete,  $360^\circ$ , in the horizontal plane. Additionally to the  $xyz$ -location of the reflecting surface point, the intensity of the received echo is registered as well.

**Other scan projects.** Only in the last years, terrestrial laser scanning is becoming popular as a measurement technique. Therefore existing literature is still sparse, both in frequency and in contents. These days however, laser scanning is more and more used for practical applications. Examples include forestry, [Pfeifer et al., 2004], tunnel monitoring, [Schulz and Ingensand, 2004], and deformation measurements of concrete poles, [Gordon et al., 2004]. In a performance comparison test of several scanners, [Böhler et al., 2003], measurement noise between 1 and 5mm were reported at a scan distance of 90m for the Leica HDS 2500, the predecessor of the scanner we used. The Leica HDS 2500 was also used to detect lock door deformation due to water pressure, [Schäfer et al., 2004]. Its measurements were compared to tachymetric measurements and differences occurred of up to 3mm. By means of the high spatial resolution of the laser measurements it turned out to be possible to detect deformations ranging from 1.5cm to 4cm on the lock doors between high and low water pressure.

**Tunnel deformation.** After digging and placement of concrete elements on tunnels walls, deformation of these tunnel elements will occur due to the weight pressure of the ground above the tunnel. Typically deformations of a few centimeters are expected. Traditionally such deformations were monitored by analyzing time series of tachymetric control point measurements. An important drawback of this method is that only deformation at a

very limited set of points can be measured and that it is not possible to obtain a complete surface model of the tunnel wall. In this article we will therefore investigate the possibilities of terrestrial laser scanning for detecting these kind of deformations. For validation purposes tachymetric point measurements are still included in the analysis. Here it should be noted that in comparison to the deformation investigations from [Gordon et al., 2004] and [Schäfer et al., 2004] the time difference between epochs will be much larger while the scanner has to be removed between two measurements as well. The focus in this article is on the accuracy analysis of one single tunnel scan and on the possibilities to join scans that are obtained from different scan points. For this purpose, three different test scans from one rectangular tunnel are analyzed together with a set of tachymetric control points. The final goal of the project however is tunnel deformation monitoring and this will be the main thread in the analysis of the results: the conclusions from the analysis in this article will be incorporated in the design of a measurement setup and in developing a change detection method for a near future tunnel deformation monitoring project.

**Paper outline** In Section 2 we discuss the theoretical background of the data analysis methods. In Section 2.1 we consider the scanner geometry, in Section 2.2 a scan registration method and in Section 2.3 the segmentation algorithm. Section 2.4 describes a deformation analysis method. In Section 3 these methods are applied on three scans of the same tunnel. Section 3.1 describes the data, Section 3.2 analyzes the data density, Section 3.3 discusses the accuracy of a single scan, Section 3.4 compares the same ceiling in different scans, while Section 3.5 combines two scans. The paper ends with conclusions.

### 2 LIST OF METHODS

#### 2.1 Point density as a function of the scan parameters.

A point hit by the scanner can be parameterized by three polar coordinates relative to the scanner: a horizontal angle  $\beta$ , a vertical angle  $\zeta$ , and a range  $R$ . Assume we have a straight tunnel, with a horizontal tunnel axis, with a rectangular, horizontal tunnel floor. Let  $h$  denote the the height of the scanner above the floor. Define rectangular local  $xyz$  coordinates by choosing one direction of the tunnel axis to be the positive  $x$ -axis, by taking for the  $y$ -axis the axis perpendicular to the  $x$ -axis in the horizontal plane, and

for the  $z$ -axis the remaining axis, oriented such that the positive direction is upwards. If the scanner emits a ray at angles  $(\beta, \zeta)$ , the floor will be hit by the ray at position  $\text{pos}(\beta, \zeta)$  given by

$$(x, y)^T = \text{pos}(\beta, \zeta) = \frac{h}{\tan \zeta} (\cos \beta, \sin \beta)^T \quad (1)$$

The scanner will emit rays at certain angular intervals  $\Delta\beta = \Delta\zeta$  of, say, 1 degree. If  $\zeta$  runs from 90 to 0 degree and  $\beta$  from  $-90^\circ$  to  $90^\circ$ , then exactly those points at the first  $15m$  of the tunnel floor will be scanned as shown in Figure 1 on the left.

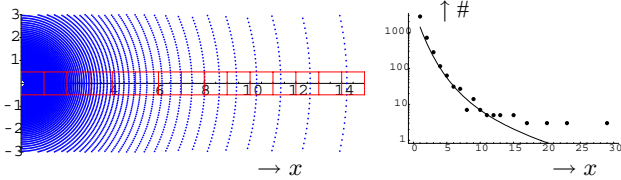


Figure 1: **Left:** points scanned. **Right:** Number of points per  $m^2$  as function of the horizontal distance  $x$  (log-scale).

Clearly, the number of points decreases rapidly with increasing distance. We quantify this by determining the number of points in  $1m^2$  square along the  $x$ -axis. Rewrite Equality 1 as

$$\beta = \arctan \frac{y}{x}, \quad \zeta = \arcsin \frac{h}{\sqrt{x^2 + y^2 + h^2}}. \quad (2)$$

An approximation  $N = n(i, h, \Delta\zeta, \Delta\beta)$  for the number of scan points in the square with vertices  $(i-1, \pm\frac{1}{2})$  and  $(i, \pm\frac{1}{2})$  is given by

$$N = \frac{2 \operatorname{atan} \frac{1}{2i}}{\Delta\beta} \frac{\operatorname{asin} \frac{h}{\sqrt{i^2 + h^2}} - \operatorname{asin} \frac{h}{\sqrt{(i-1)^2 + h^2}}}{\Delta\zeta} \quad (3)$$

where  $i$  denotes the maximal  $x$ -coordinate of the square.  $n(i, h, \Delta\zeta)$  approximates the number of hits per square by counting the number of times the scan angle interval fits in a square. The points in Figure 1, on the right, give the number of points per red square, while the continuous line through the points plots Equation 3 for  $\Delta\theta = 1$  and  $h = 2$ . The difference between graph and points at higher distances is due to the discreteness of the scan points.

## 2.2 Registration with ICP

For transforming the different scans into one superior coordinate system we used the Iterative Closest Point (ICP) method [Besl and McKay, 1992]. It works on two scans, transforming the point cloud of the second scan into the coordinate system of the first. In the implementation used, the corresponding (closest) point in the first scan is computed for every point of the second scan, and the distance within each point pair is used for sorting the correspondences. The correspondences with the shortest distances, specified by a fixed percentage, e.g. 20%, are used to determine the six transformation parameters (shift and rotation) for minimizing the distance between corresponding points. Iteration end is declared, if the sum of squared distances does not become smaller anymore.

## 2.3 Segmentation

Segmentation groups points, which have under a given homogeneity criterion similar properties, into segments. A short overview on segmentation can be found in [Vosselman et al., 2004]. The method applied here follows

the region growing approach for extracting planes. First, in each point an initial normal vector is estimated from its neighbors by fitting of a plane. Points with a large r.m.s.e. are discarded from the beginning, because they are more likely to be single points, or on surfaces with a very small extent. Planes are grown, starting with the initial normal vector and position of the seed point. Neighboring points are accepted if they are i) below a threshold distance to this plane, and ii) the angle between plane normal vector and initial normal vector is below a threshold. After adding a point, the plane is determined anew by adjustment of all accepted points. If no more points can be added to a segment, the next segment is initiated with a new seed point. An example of the segmentation for one scan can be seen in Fig. 2.

## 2.4 Deformation analysis.

The strong point of terrestrial laser measurements in comparison to e.g. tachymetry is the large number of measurements that is automatically generated. A disadvantage though, is that it is difficult to assess some fixed benchmarks, like bolts. In order to profit in an optimal way from this large number of observation it is favorable, not to try to detect deformation of single points of lines, but rather to model surface segment deformation. Assume we have obtained laser scans of the tunnel surface in distinct epochs. After the registration and segmentation steps as described above we may assume that we can compare corresponding surface elements of the distinct epochs. Moreover the point density analysis makes it possible to assure in the measurement design that enough scan points per surface element are available.

Think for example of a tunnel that is extended, during construction, by a series of tunnel segments that together form a cylindric extension of the tunnel. Assuming the scan density to be sufficient, one can model one such cylinder and thereafter consider deviations of the measurements from the cylinder model. By looking at this residuals it may well be possible to test whether single tunnel segments are well-placed or deformed.

In a next step the so-called Delft method of deformation analysis, [Verhoef, 1997], can be applied to analyze whether one cylinder is stable in time. For this purpose both a functional and stochastic model is designed. The functional model describes the expected functional relation between observations and the cylinder model as a function of time. the stochastic model describes the uncertainties in the observations. Except for stability one often tests for outliers or for easy, low number of parameters, kinematic models. In our case, for example, it is obvious to model the expected deformation due to the pressure of the ground above the tunnel. Different functional models can be compared in a testing procedure, that takes the observation redundancy into account together with the stochastically scaled deviations from the observations to the distinct functional models.

As will be shown in the data analysis part, a large number of observations enables us to consider a complete distribution of the residuals between observations and model. Empirical distributions that look 'nice', give greater confidence in the applied functional model. On the other hand, deviations from the expected distribution can be used to adapt the functional model in a specific direction.

## 3 DATA ANALYSIS

### 3.1 On the tunnel data.

In this section we analyze scan data from a tunnel in Rotterdam, obtained by the Leica HDS3000 scanner. The tunnel has a width of about 6m, is about 100 meters long, has rectangular walls and contains a rather gentle curve. Three different scans are available,

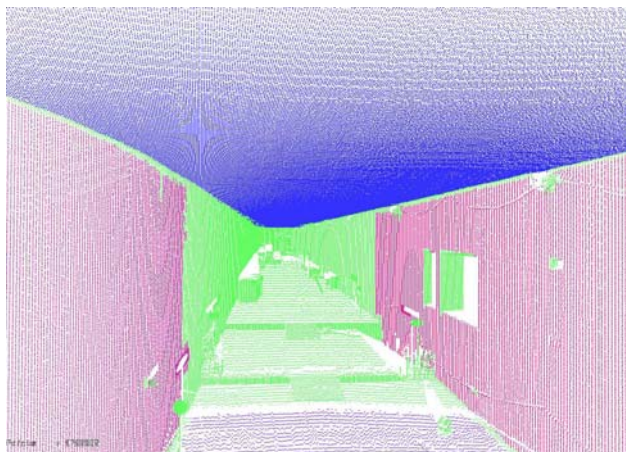


Figure 2: Segmentation of a tunnel scan. Four segments are distinguished, two on the sides, one on the bottom and one big ceiling segment. The remaining points were not classified as belonging to a segment, as the minimum segment size was set at 10 000.

numbered 4, 5 and 6, consisting of 3.8, 2.8 and 3.5 million points each. Scans 4 and 5 were obtained from approximately the same position, while for scan 6 the scanner was moved by about 20m. The orientation of the three scan positions with respect to the horizontal plane was comparable, within some margin of  $10^\circ$ . For every scan seven point parameters are available, a  $xyz$  position within the local coordinate frame, an intensity value and three RGB-coded color values. Except for the scans, some 29 tachymetric control points were measured as well.

The analysis of the scans has been concentrated on the ceiling. The part of the ceiling that has been scanned is very elongated, compare also Figure 2. This made it possible to analyze a complete range of scan distances, from 1m to 50m, and scan beam incidence angles, from almost perpendicular to almost horizontal, within one segment: this ceiling can be considered a plane, which gives us a easy model that simplifies the data analysis procedures.

### 3.2 Point density in practice.

First we will consider if the point density in practice matches the values as found in section 2.1. After a segmentation step we obtained from scan 5 a segment consisting of ca. 450 000 of the total of 2 800 000 points. Figure 3 shows the histogram of the distances to the scan position of the points in the segment. It turns out that the found histogram matches the expected number of points at a given distance according to Equation 3. This expected number is indicated by the grey line. The deviations between the histogram and the grey line are probably due to the fact that the ceiling is not perfectly planar, as we will see later. On short distances there is a strong scan-shadow effect, because the scanner is not able to scan directly around itself.

This analysis shows that it is feasible to estimate the expected number of points on forehand. This is important in designing the measurement setup as in this way it can the locations of the scan positions can be optimized with respect to the necessary minimal number of scan hits per surface area. It should be noted however, that in areas featuring complicated objects, points may get lost due to masking effects.

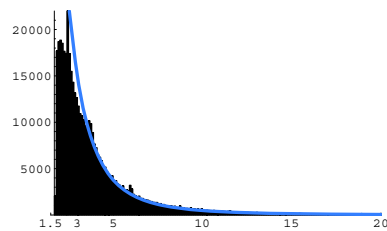
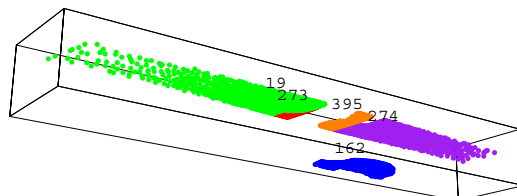


Figure 3: Histogram of the distances of the scan points to the scanner. The grey line indicates the theoretical number of scan points, according to Equation 3.



Relative positions of the five segments

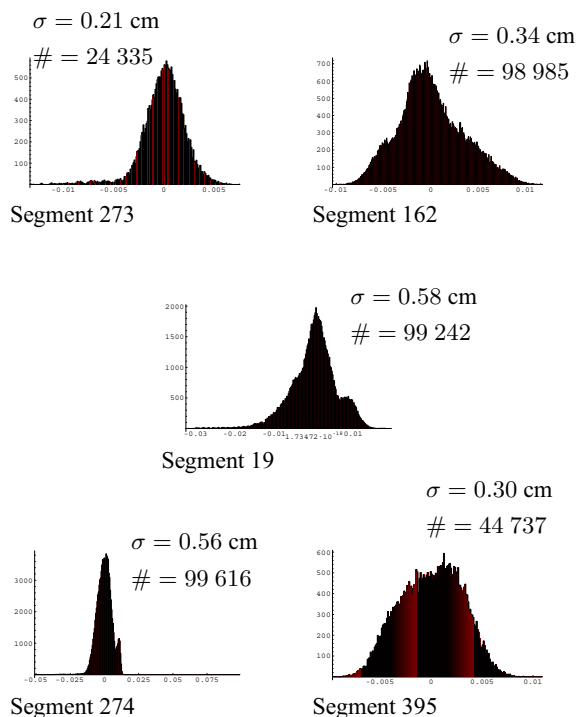


Figure 4: Relative positions, histograms and standard deviations of the five segments.

### 3.3 Scan segmentation results.

Segmentation of scan 5 results in five big segments, four at the ceiling and one on the floor. For each of these five segments the best fitting least squares plane was determined together with the residuals between the scan points classified as belonging to the segment and the segment itself. The number of points per segment, the histograms of the residuals, and the standard deviation of the least squares adjustment are shown in Figure 4. The his-

tograms show that in general the residuals are not distributed normally. This would imply that modeling the segments as planes is doubtful, or that the parameters used for the segmentation algorithm were too tolerant. But, on the other hand, all standard deviations found are below 6mm and it is expected that the measurement noise is even lower. The residuals for segment 273 seem to be normally divided, and in this case the standard deviation only amounts to 2mm. This segment, however, is the smallest considered and is positioned close to the scanner.

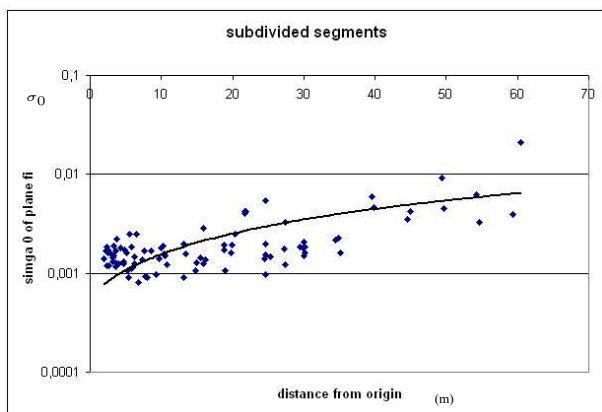


Figure 5: Accuracy of the planar adjustment as a function of the distance of the plane to the origin.

For a more local analysis, every segment is subdivided into sub-segments of about 2m by 4m. Again, for every subsegment a best fitting least squares plane is determined together with the a posteriori standard deviation  $\sigma_0$  of the adjustment. If it is assumed that these small segments correspond to planar ceiling pieces in reality as well, this adjustment-accuracy will give us exactly the measurement accuracy. Figure 5 shows the standard deviations per planar segment against the distance of the planar segment to the origin. This distance is defined as the distance of the center of gravity of the segment points to the scanner origin. From the plot we conclude that

- the local planar adjustment accuracy is in between 1mm and 1cm;
- the local planar adjustment accuracy decrease with distance. This may be due to the decreasing angle on incidence of the laser pulse on the ceiling with increasing distance. This causes an enlargement of the pulse footprint corresponding to a reduction of the measurement accuracy.

Figure 5 can be used to determine a maximal scan distance, given a certain required accuracy threshold. The black regression line relates the found values for accuracy to the distance. If, for example, a standard deviation value of  $\sigma = 3\text{mm}$  is required, then the regression line suggests that the maximal distance for scanning should not exceed 30m.

#### 3.4 Spatial distribution of the plane model residuals.

In this section we compare residuals obtained from three different scans of the same ceiling. That is, assuming the tunnel ceiling to be planar, we obtain a set of residuals from the planar adjustment, after segmentations, for each of the scans 4, 5 and 6. We examine if the three sets of residuals obtained in this way are comparable, in the sense that the spatial distribution patterns of the residuals display the same features.

The ceiling as determined from the data is displayed in Figure 6. For scans 4 and 6 the ceiling corresponds to exactly one segment, as found by the segmentation algorithm, while in the case

of scan 5 four segments belonging to the ceiling are found. This division into multiple segments is caused because the maximal segment size limit in the software is smaller than the number of ceiling points, in the case of scan 5. This problem also explains why some ceiling parts are missing in this case. Other ceiling holes however are caused by actual features in the tunnel that mask the ceiling from the scanner or by limitations of the scanner range.

The color of the points in Figure 6 encodes the size of the residual from the best fitting plane adjustment. For every scan such a plane is determined. Blue points are points that are more than 1 cm below the plane, while red points are at least 1 cm above the plane. For every scan, the number of points, the maximal deviations and the planar-fit accuracy are given in the following table:

Scan	# ceiling points	Max. deviation	RMSE
4	134 698	54 mm	7.3 mm
5	267 930	109 mm	6.5 mm
6	95 738	149 mm	7.3 mm

It is clear at first sight that the same characteristics, the typical ovals, show up in all scans. Scans 4 and 6 were obtained from approximately the same position and demonstrate the same 'deformations', that is, deviations from the planar fits, upto a few decimeters. Even scan 5, although obtained from 20 m further on, displays the same deformation pattern. This proves that the colored ovals are characteristic to the ceiling and are not caused by some systematic error in the laser measurements. Moreover, the deviations found are larger than 1 cm. Simultaneously, measurement noise, due to random measurement errors, is visible as well. As there are large areas having a deviation of more than 1 cm, we conclude that the ceiling is not a flat ceiling. The average least square error found is about 7 mm, but as we concluded that the ceiling is not flat, we may assume that the scanner accuracy is better than 7 mm.

#### 3.5 Registration and comparison of the three scans.

The next step is to directly compare scans obtained from distinct scan positions. This is only possible after the scan data of the different scans are converted in a common coordinate system. For this we use the ICP method as described in the Methods section. Therefore we assume from now on that all our scans are registered. Given are, as before, the points reported to belong to the ceiling of scan 4. These points are triangulated in such a way that a complete 3D surface existing of triangles is obtained. Then for every ceiling point of scan 5, after registration, the vertical distance to this surface is determined. If the ceiling would be perfectly flat and if no measurement errors would occur, then these differences would all be equal to zero. The distribution of the vertical distances are given in Figure 7. Distances ranges from -0.199m to 0.253 meter. The first and third quantile are close to 0mm and 3mm, respectively, which shows that the differences are close to the expected difference of 0mm. The values for the mean, 2.3 mm and the median, 2mm, indicate a small systematic shift. The standard deviation of the vertical distances is 6mm.

At first sight these figures point to a systematic deviation of 2mm and an accuracy of 6mm. This is too pessimistic however. As can be seen in Figure 7, left, the modulus of the histogram occurs at +1mm and not around 2mm, like the median and the mean. The distribution is asymmetric, having a long tail at the positive side. From considering the spatial distribution of the vertical distances, see Figure 7, top right. It follows that larger differences occur near certain features, like near the hole in the middle. This is

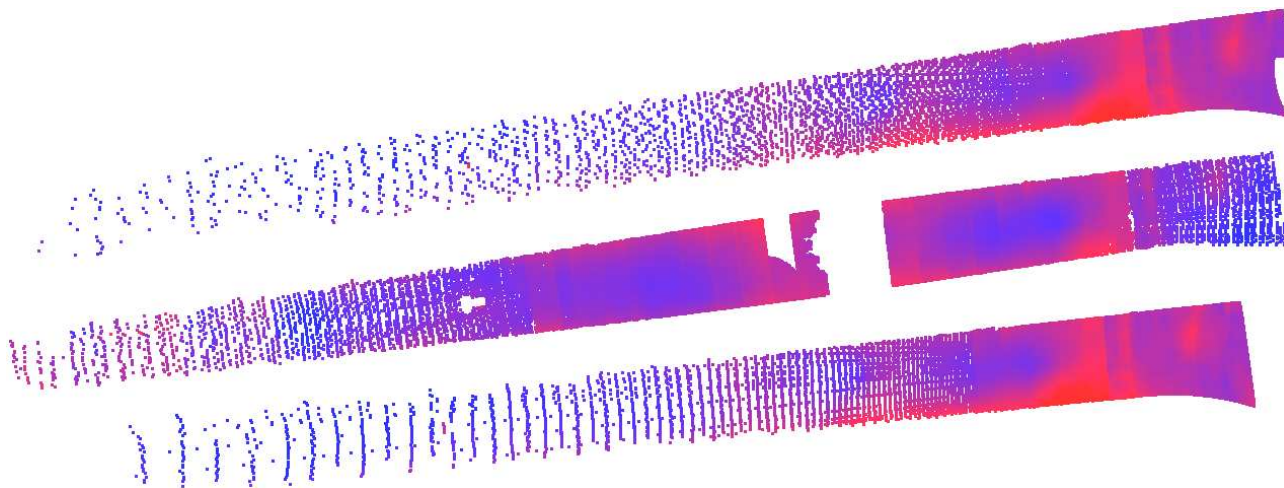


Figure 6: Ceiling from Scan 4, below, Scan 5, in the middle and Scan 6, above. Blue points are more than 1cm below the adjusting plane, red points more than 1cm above. The purple colors are determined by means of linear interpolation.

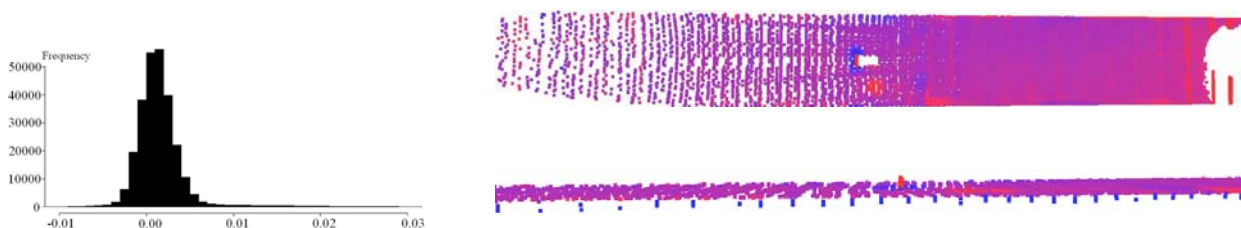


Figure 7: Left: distribution of the vertical distances between the points belonging to the ceiling in scan 5 and scan 4 after registration. A lag width of 1mm was used in the histogram. The unit of the horizontal axis is meter. Top Right: Spatial distribution of the vertical distances between Scan 5 and Scan 4. Values below -2cm are colored blue, values above +2cm are colored red. Values in between are interpolated linearly. Bottom right: Side view of the vertical distances between Scan 5 and Scan 4. Big differences (-20cm and +25cm) occur near small objects, measured in one scan, but missed in the other scan, like near the ceiling 'hole' and near certain features in the wall.

more clear in the side view, Figure 7, bottom right. Other larger distances occur near the bulges between the plates of the ceiling and near the boundary of the ceiling.

This is to be expected: even small differences in the scan position for different scans will cause larger deviations near features where the ceiling topography is changing, as not exactly the same points are measured. Even smaller deviations are introduced by our triangulation method due to the bowl that we observed in the middle of the ceiling. This could be an explanation for the systematic error of 1mm. Also the ICP algorithm does not guarantee that only points from distinct surface segments are used for registration. For the moment we should note this remaining error and incorporate it in the variance covariance structure of a deformation analysis.

While incorporating the above discussion and the asymmetry of the distribution of the vertical distances and its possible explanations, we conclude that the scanner accuracy, even when operating from different scan positions (!) is within 6mm. A visual interpretation of the left tail of the distribution in Figure 7 suggests a standard deviation of about 3-4 mm. Three circumstances should be considered together with this conclusion.

1. The relative orientation is determined by means of the ICP algorithm and not by using control points. In a tunnel deformation

scenario, no identity between surfaces can be assumed requiring the use of control points in a superior coordinate system.

2. The two scan positions were about 20m apart, causing systematic effects at the boundaries of surfaces, because some protruding objects were measured in one scan but masked in the other scan. By comparing scans obtained from more close scan positions, more insight in the accuracy could be obtained.

3. Even in the case of close by scan position, the triangulation method will introduce deviations in case the modeled surface is not perfectly flat, as there is no 1-1 correspondence between vertices (scan point positions) of different scans.

#### 4 CONCLUSIONS AND FURTHER RESEARCH

In this paper we analyzed three terrestrial laser scans from the same tunnel, keeping in mind that a final aim is to detect deformation in the construction stage of a newly built tunnel. From our analysis we draw the following conclusions.

**Measurement accuracy.** • Leica claims a accuracy of 6mm at 50m for the Leica HDS 3000. Within one scan we find accuracies ranging from 2mm at 10m to 6mm at 50m scan distance by applying a segmentation method and by analyzing ceiling segments

that are supposed to be flat. • Analysis of the spatial distributions of the residuals of a model fits is a useful method to detect small features or big features with small deviations on one hand and to compare different scans on the other hand. • Moreover we show that it is possible to combine scans obtained from different scanner positions after using an ICP registration resulting in a maximal systematic error of 2mm and a standard deviation of less than 6mm.

**Prospect of deformation monitoring.** • It is possible to predict the measurement density at a given range. This makes it possible to design a measurement setup such that objects that have to be monitored, are scanned by sufficient points. • It is possible to combine scans obtained in different epochs from different scan positions in one deformation analysis method. It is advisable though to use a control point based registration method. • To optimally profit from the high redundancy of terrestrial laser altimetry a deformation analysis method should be based on smooth surface models. Points can be classified into different surface objects by using a segmentation algorithm.

**Acknowledgments.** Gemeentewerken Rotterdam is thanked for initiating this research, for their comments and for providing us with the data.

#### REFERENCES

- [Besl and McKay, 1992] Besl, P. and McKay, N., 1992. A method for registration of 3D shapes. *IEEE Transactions on Pattern Analysis and Machine Intelligence* 14(2), pp. 239–256.
- [Böhler et al., 2003] Böhler, W., Bordas Vicent, M. and Marbs, A., 2003. Investigating laser scanner accuracy. *The International Archives of Photogrammetry, Remote Sensing and Spatial Information Sciences XXXIV(Part 5/C15)*, pp. 696–701.
- [Gordon et al., 2004] Gordon, S., Lichti, D., Franke, J. and Stewart, M., 2004. Measurement of structural deformation using terrestrial laser scanners. In: *1st FIG International Symposium on Engineering Surveys for Construction Works and Structural Engineering*, Nottingham, United Kingdom.
- [Pfeifer and Litchi, 2004] Pfeifer, N. and Litchi, D., 2004. Terrestrial laser scanning. *GIM International*.
- [Pfeifer et al., 2004] Pfeifer, N., Gorte, B. and Winterhalder, D., 2004. Automatic reconstruction of single trees from terrestrial laser scanner data. In: *ISPRS, Vol. XXXV, Istanbul, Turkey*.
- [Schäfer et al., 2004] Schäfer, T., Weber, T., Kyrinovic, P. and Zamecnikova, M., 2004. Deformation measurement using terrestrial laser scanning at the hydropower station of Gabčíkovo. In: *INGEO 2004 and FIG Regional Central and Eastern European Conference on Engineering Surveying*, Bratislava, Slovakia.
- [Schulz and Ingensand, 2004] Schulz, T. and Ingensand, H., 2004. Terrestrial laser scanning - investigations and applications for high precision scanning. In: *Proceedings of the 'FIG Working Week - The Olympic Spirit in Surveying'*, Athens, Greece.
- [Verhoef, 1997] Verhoef, H. M. E., 1997. Geodetische deformatie analyse. Lecture notes, Delft University of Technology, Faculty of Geodetic Engineering, in Dutch.
- [Vosselman et al., 2004] Vosselman, G., Gorte, B., Sithole, G. and Rabbani, T., 2004. Recognising structure in laser scanner point clouds. *International Archives of Photogrammetry, Remote Sensing and Spatial Information Sciences* 46(part 8/W2), pp. 33–38.